

Vision-based Large-scale 3D Semantic Mapping for Autonomous Driving Applications

Qing Cheng¹
qing@artisense.ai

Niclas Zeller^{1,3}
niclas.zeller@h-ka.de

Daniel Cremers^{1,2}
cremers@tum.de

Abstract—In this paper, we present a complete pipeline for 3D semantic mapping solely based on a stereo camera system. The pipeline comprises a direct sparse visual odometry front-end as well as a back-end for global optimization including GNSS integration, and semantic 3D point cloud labeling. We propose a simple but effective temporal voting scheme which improves the quality and consistency of the 3D point labels. Qualitative and quantitative evaluations of our pipeline are performed on the KITTI-360 dataset. The results show the effectiveness of our proposed voting scheme and the capability of our pipeline for efficient large-scale 3D semantic mapping. The large-scale mapping capabilities of our pipeline is furthermore demonstrated by presenting a very large-scale semantic map covering 8000 km of roads generated from data collected by a fleet of vehicles.

Index Terms—3D mapping, autonomous driving, semantic segmentation, visual SLAM.

I. INTRODUCTION

Autonomous Driving (AD) is among the major technical challenges pursued by automotive companies and academics around the globe. One of the most considerable obstacles on the way to full autonomy is the challenge of 3D perception: understanding the 3D world around the vehicle with its various sensors. An autonomous vehicle (AV) can perform online path planning and make reliable, safety-critical decisions based on such an established environmental model.

While in the past reliable perception was enabled by equipping a vehicle with all different kinds of sensor modalities, today's trends go more towards the use of fewer and cheaper sensors to perceive the surrounding of a vehicle.

State of today, in addition to online perception, environmental models are complemented by topological information of static road furniture. High-definition maps (HD maps) can provide such redundant and abundant information to back up the online sensor data. Nevertheless, it is crucial to keep such maps up to date due to rapid changes in road infrastructures, especially in urban environments. Hence, instead of expensive mapping sensors and manual labeling processes, lightweight and scalable online mapping pipelines become more preferred.

In this paper, we are proposing a complete vision-based pipeline towards the goal of creating scalable and up-to-date maps. Our pipeline generates 3D semantic maps at scale from only a stereo-vision system, as shown in Figure 2.

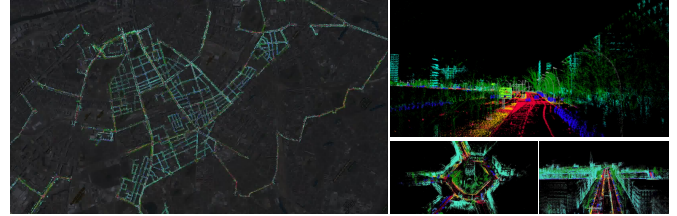


Fig. 1: **Large-scale semantic map of Berlin.** *Left:* We generated a large-scale semantic map covering 8000 km of roads in Berlin with a fleet of vehicles. *Right:* Zoomed-in sections of the semantic map show the fine-grained 3D reconstruction details of the map.

We believe that the proposed pipeline reveals the potential of purely vision-based mapping systems for autonomous driving applications and can be extended towards extracting information like lane markings, etc., although it does not provide fully vectorized HD maps yet. In Figure 1, we demonstrate that our method can be used to create city-scale maps based on a fleet of vehicles.

Our Contributions in detail are the following:

- A fully automatic vision-based 3D mapping pipeline that can create large-scale 3D semantic maps efficiently.
- A simple but effective temporally consistent point labeling scheme that improves the accuracy of the 3D point labels by taking the structural information provided by the visual odometry front-end into account.
- A benchmark for vision-based 3D semantic mapping pipelines, which fuses 3D LiDAR and 2D image ground truth labels.

II. RELATED WORK

In this paper, we are presenting a pure vision-based semantic mapping pipeline. Therefore, there are basically two different research streams to which our method relates. One is visual SLAM, which allows building large-scale 3D maps only from image data. The other is semantic segmentation, which aims to extract semantic information from the captured sensor data. Hence, in the sequel, we review both the state of the art in visual SLAM as well as in 2D (image-based) and 3D (LiDAR-based) semantic segmentation. Furthermore, we discuss related mapping pipelines based on different sensor modalities. For all these tasks, there exists several popular datasets relevant for training and benchmarking [2], [3], [1], [4], [5], [6], [7].

¹ Artisense GmbH

² Technical University of Munich

³ Karlsruhe University of Applied Sciences

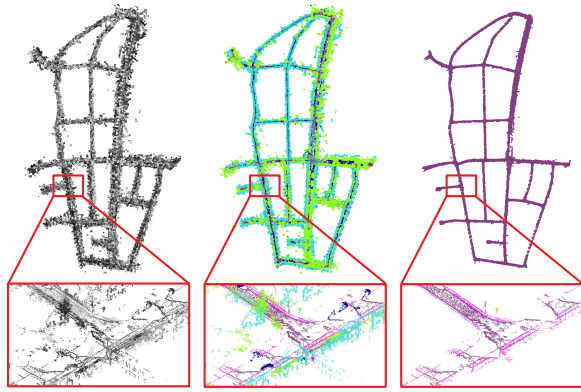


Fig. 2: **3D semantic map** generated by the proposed pipeline for sequence 0 of the KITTI-360 dataset [1]. **Left:** Sparse point cloud generated from direct visual odometry (VO). **Center:** Semantic 3D point cloud. **Right:** Extracted street-level information, including roads, sidewalks, traffic signs/lights. Due to the high accuracy and quality, the generated semantic map can be used to perform further vectorization towards HD map generation.

1) *Visual SLAM:* or structure-from-motion (SfM) algorithms are at the core of any mapping pipeline. These methods can be mainly divided into indirect (or keypoint-based) and direct approaches.

Indirect approaches extract a set of interest points from the image and then perform pose and 3D point estimation by formulating a geometric energy term using the extracted interest points [8], [9], [10], [11], [12], [13]. Here correspondences of interest points between consecutive images are either established by matching descriptors [8], [9] or based on optical flow estimation [12]. While indirect methods generally provide high tracking robustness, the 3D reconstruction is limited to the sparse set of interest points, making it insufficient for 3D mapping purposes. This can be overcome by combining an indirect pose estimation with multiple-view stereo (MVS) [14], [15], [16].

Direct approaches skip the keypoint extraction step and perform optimization directly based on pixel intensities [17], [18]. As these methods generally make use of much more image points than indirect approaches, they can provide a richer and more detailed 3D reconstruction of the environment [17], [18], [19]. Direct methods do not establish any point-to-point correspondences between images as done in indirect approaches, so they tend to be less robust under very fast motion and rapidly changing lighting conditions. In [20], this problem is tackled by integrating predictions from a deep neural network (DNN) into a direct SLAM formulation. While tasks like loop closure detection and relocalization, in general, are very challenging for direct approaches due to the non-repeatable selection of points, [21], [22] have shown that this bottleneck can be overcome by integrating detected keypoints into a direct SLAM system. In contrast to SLAM approaches which are designed for online operation and sequential image data, SfM tackles the problem in a more general way by performing 3D reconstruction from a set of unordered images [23], [24].

2) *Semantic Segmentation:* is known as the task of assigning a semantic class label to each recorded data point (e.g.

image pixel or 3D LiDAR point). In recent years, research in this field is heavily driven by large-scale datasets [3], [1], [4], [5], [6]. Two main work streams are present for semantic segmentation in robotic and autonomous driving use-cases: 2D semantic segmentation on RGB or intensity images and 3D semantic segmentation on structural 3D representation, e.g. LiDAR point clouds.

Due to the high resolution of images and the rich textual information, image-based approaches provide high-quality segmentation results [25], [26], [27]. In general, these methods are highly efficient using 2D CNNs. The pioneering work [25] tackles the semantic segmentation task with a fully convolutional neural network (FCNN) which can generate a full-resolution semantic mask for an input image of arbitrary size. To utilize more high-level context, [28], [29], [30], [31] integrate the probabilistic graphical models, e.g. Conditional Random Fields (CRFs), into their network architectures. Another direction is to exploit multi-scale inputs [32], [33], [34], [35] or spatial pyramid pooling [36], [27], [37], [38] in order to generate feature maps encoding contextual information from different resolutions for the final pixel-level classification. The popular encoder-decoder architectures learn dense semantic features from the encoded low-resolution feature responses from single or multiple encoder layers and demonstrate promising performance on semantic segmentation tasks with this scale context [39], [40], [41], [42], [43], [44]. Attention mechanisms are also introduced to semantic segmentation architectures which outshine max and average pooling with the selective aggregation of various contextual features [33], [45], [46], [47], [48], [49]. Auto-labelling techniques [50], [51], [48] and domain adaptation methods [52], [53] are also proposed to alleviate the reliance on the expensive pixel-wisely labeled training data. In our work, we make use of the work proposed by [50], which demonstrates state-of-the-art performance in automotive environments.

LiDAR-based 3D segmentation approaches commonly rely on the geometric point distribution to predict semantic point labels. One of the main challenges for these approaches is the unstructured nature of the 3D point cloud. This challenge can be tackled by transforming the point cloud e.g. into a range image representation and applying classical 2D CNNs [54], [55]. To better utilize the 3D nature of point clouds, [56] proposes to apply 3D CNNs to a voxel representation obtained from the point cloud.

3) *Semantic Mapping:* While the approaches presented in Section II-2 solely focus on the segmentation problem using individual images or individual LiDAR scans, we understand the task of semantic mapping as the combination of segmentation, localization and mapping.

In [57], dense 2D semantic mapping is performed by projecting class labels from street view images onto the ground plane. Furthermore, in [58] an extension to [57] is proposed, which performs dense reconstruction from stereo images and labels the resulting 3D model based on image segmentation results.

Instead of using only image data, the methods proposed

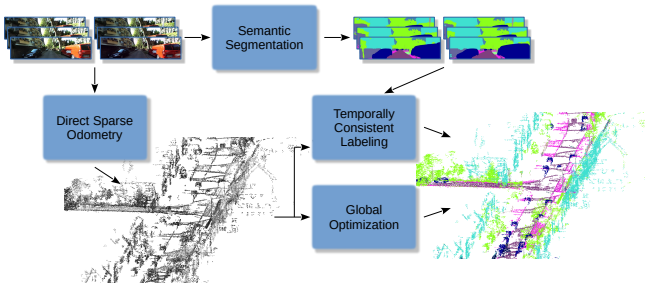


Fig. 3: **Semantic Mapping Pipeline.** A direct VO front-end estimates relative camera poses and a sparse 3D reconstruction of the environment based on a sequence of stereo images. A segmentation module predicts dense 2D semantic labels for the stereo camera images selected as keyframes by the VO. Based on the VO outputs and the 2D semantic labels, temporally consistent 3D point labels are generated. Global optimization can be applied to compensate for drift based on loop closure detection and the integration of RTK-GNSS measurements if available.

in [59] and [60] make use of a LiDAR sensor for 3D map generation and perform semantic image segmentation to label the 3D points. The work presented in [61] also makes use of LiDAR-based 3D reconstructions and image-based segmentation to reconstruct both 3D semantic point clouds as well as semantic 2D occupancy grids.

III. LARGE-SCALE 3D SEMANTIC MAPPING

The proposed 3D semantic mapping system utilizes solely stereo images and optional sensor data like GNSS (Global Navigation Satellite System) for global positioning and IMU measurements. Figure 3 shows an overview of our semantic mapping pipeline. The direct VO module of our pipeline estimates relative camera poses and a sparse 3D reconstruction of the environment (Sec. III-A). Global map optimization is performed based on loop closure detection. If available, RTK-GNSS measurements are integrated to obtain a geo-referenced and globally accurate map. A state-of-the-art semantic segmentation network (Sec. III-B) is used to generate accurate semantic labels for each pixel of the stereo images corresponding to the keyframes defined by the VO front-end. Furthermore, our temporally consistent labeling module can generate temporally consistent 3D point labels based on the VO outputs and the 2D semantic labels (Sec. III-C). When lifting the 3D reconstruction to a global, geo-referenced, frame with GNSS data, a city-scale map can be created by stitching together the reconstructions from a fleet of vehicles, as shown in Figure 1.

A. Visual Odometry and 3D Mapping

The core of the proposed semantic mapping pipeline is a state-of-the-art visual SLAM algorithm. To provide rich information about the 3D environment, a detailed reconstruction of the surroundings at a certain density level is required. The proposed semantic mapping pipeline relies on a direct SLAM front-end for 3D map generation, which provides a much denser and more detailed reconstruction of the environment compared to indirect (keypoint-based) SLAM approaches.

Namely, we make use of a direct sparse SLAM formulation working on stereo images, as proposed in [19]. Here, in a local photometric bundle-adjustment, six degrees of freedom (6DoF) poses are estimated jointly with a sparse 3D reconstruction of the environment and optimized with respect to a photometric energy function:

$$E = \sum_{i \in \mathcal{F}} \sum_{\mathbf{p} \in \mathcal{P}_i} \left(\left(\sum_{j \in \text{obs}^t(\mathbf{p})} E_{ij}^{\mathbf{p}} \right) + \lambda E_{is}^{\mathbf{p}} \right). \quad (1)$$

In eq. (1), \mathcal{F} is the set of all keyframes in the optimization window and \mathcal{P}_i is the sparse set of points hosted in keyframe i . A point $\mathbf{p} \in \mathcal{P}_i$ is defined by its fixed 2D pixel location in the image and an inverse depth d which is estimated during optimization. $\text{obs}^t(\mathbf{p})$ defines the projections of the point \mathbf{p} to the left images of all other keyframes in the optimization window. Furthermore, $E_{is}^{\mathbf{p}}$ defines an additional photometric energy term based on the projection of a point \mathbf{p} into the corresponding right image. For further details, we refer to [18], [19].

Furthermore, our VO system additionally is able to tightly integrate inertial measurements from an inertial measurement unit (IMU) if available, as described in [62]. By fusing the VO outputs with GNSS measurements and performing loop closure detection, a globally consistent 3D map is obtained. Overall, the mapping front-end used in our pipeline is similar to the one proposed in [7].

B. Semantic Segmentation

Semantic segmentation plays an influential role in our pipeline as it sets the baseline for the quality of our semantic point clouds. Since there are already plentiful excellent works, we build our pipeline based on them. Because of the modularity of our pipeline, the semantic segmentation component consumes only images and, thus, is independent of the rest of the pipeline. Therefore, any start-of-the-art method can be integrated into our pipeline.

In this paper, we build our pipeline based on [50]. The work proposed in [50] has the best performance on the KITTI semantic segmentation benchmark [63] among all open-source submissions. It achieves state-of-the-art performance by augmenting the training set with synthesised samples generated by the joint image-label propagation model along with the boundary label relaxation strategy to make the model robust to noisy boundaries.

In our pipeline, the semantic segmentation module predicts a full-resolution semantic map for each pair of images from the stereo cameras corresponding to the keyframes defined by the VO module and then feeds the consecutive maps into the temporally consistent labeling module (Section III-C).

C. Temporally Consistent Labeling

Even though DNNs for image-based semantic segmentation significantly improved over the last years, these networks still suffer from noise in the predicted labels as well as temporal inconsistency across the estimations of a temporal sequence of images. On one side, there are usually significant

appearance changes of objects caused by the perspective imaging process. On the other side, the prediction capability of DNNs is still developing and imperfect estimations can often be temporal inconsistent.

However, with respect to the task of autonomous driving, one is generally more interested in temporally consistent 3D semantic labels than 2D labels in image space. Therefore, we are proposing a simple but effective scheme to obtain accurate and consistent 3D labels only from images.

As described in Section III-A, our direct sparse VO system [18], [19] generates a sparse set of points $\mathcal{P} := \{\mathcal{P}_0, \mathcal{P}_i, \dots, \mathcal{P}_N\}$ to define the 3D reconstruction. Here a point $\mathbf{p} \in \mathcal{P}_i$ is defined by the pixel coordinates (u, v) in its host keyframe $i \in \mathcal{F}$ as well as a corresponding inverse depth d . Therefore, a point can be projected to a global 3D frame using the corresponding keyframe pose $\xi_i \in \mathfrak{se}(3)$. In general, the tracked points are treated as statistically independent from each other. Furthermore, the point selection scheme avoids having multiple image points hosted in different frames corresponding to the same object points.

In the segmentation process described in Section III-B, the individual images of the sequence are treated independent from each other. While the direct VO front-end implicitly establishes correspondences between consecutive images as defined in eq. (1). Therefore, we can resort to these correspondences to improve the quality of the 3D point labels.

Similar to the photometric energy formulation in eq. (1), we project each point $\mathbf{p} \in \mathcal{P}_i$ from its host keyframe i to the left images corresponding to all other keyframes j in the neighborhood in which the point \mathbf{p} is visible ($j \in \text{obs}^t(\mathbf{p})$) to generate a set of co-visible points corresponding to this point. We also project this set of left image points to their respective right images to obtain another set of corresponding points. Both sets of points from the left and right image stream constitute the final co-visible point set. Then we define a set of C votes $V := \{v_1, v_2, \dots, v_C\}$ for each point \mathbf{p} , where v_c is defined as an accumulated vote based on the weights w_j from all co-visible points for one semantic class c and C is the total number of classes.

$$v_c = \sum_{j \in \mathcal{Q}} w_j \quad w_j = \begin{cases} d_j & \text{for } c = L_j(\mathbf{q}_j) \text{ and } d_j < \text{dist}_{\min}^{-1}, \\ 0 & \text{otherwise.} \end{cases} \quad (2)$$

Here \mathcal{Q} is the set of all co-visible points, including the point \mathbf{p} itself, d_j is the inverse depth of a point \mathbf{q}_j and L_j is the 2D semantic map corresponding to keyframe j . dist_{\min} defines a minimum object distance. By utilizing the inverse depth d_j as a weighting factor for the corresponding vote, we consider the fact that predictions for points far from the camera are generally less accurate than close points. Meanwhile, image regions for very close objects commonly suffer from significant motion blur and strong perspective distortion, which again results in inaccurate predictions. This is accounted for by setting a minimum distance threshold dist_{\min} in the voting process.

Based on the set V , the point \mathbf{p} gets the label with the highest weight assigned:

$$L_i(\mathbf{p}) \leftarrow \arg \max(V) \quad (3)$$

In this way, point labels are obtained in consideration of the temporal semantic segmentation information. As the VO front-end provides only a sparse set of points, the temporally consistent labels are also only provided for this set.

D. Semantic 3D Point Cloud Generation

The final step of our pipeline is to generate the semantically labeled 3D point cloud. Based on the modules presented in Section III-B and Section III-C, we are able to assign semantic labels to points generated by the VO (Sec. III-A). Finally, these labeled 2D points are projected to 3D and transformed to a globally consistent 3D frame forming a sparse 3D semantic map as the example shown in Figure 2.

IV. EXPERIMENTS

In the following, we evaluate our pipeline on the KITTI-360 dataset [1]. We propose the generation of improved ground truth semantic labels for the generated 3D points by fusing labels of 2D images and 3D LiDAR points from the KITTI-360 dataset. We show both quantitative and qualitative results and demonstrate the performance improvement with the temporally consistent labeling. In addition to the systematic evaluations on the KITTI-360 dataset, Figure 1 shows the capability of our pipeline to generate a city-scale semantic map from data collected by a fleet of vehicles.

A. Dataset

KITTI-360 [1] is a large-scale dataset that covers 74 km suburban traffic scenes with over 400k images and over 100k LiDAR scans. It provides rich annotations, including manually labeled 3D LiDAR point clouds and front-view 2D semantic labels transferred from the 3D annotations.

As described in Section III-A, our 3D mapping core generates sparse point clouds only from images [19]. The 3D points generated by our pipeline differ from the LiDAR points provided in the KITTI-360 dataset. Hence, it is necessary to associate our generated points with the ground truth provided by the KITTI-360 dataset. Then we can properly evaluate the performance of our semantic mapping approach.

Our pipeline generates point clouds solely from image data without integrating global measurements like GNSS. Therefore, we cannot guarantee that our 3D model can be globally aligned with the provided LiDAR points up to centimeter accuracy, even though the VO front-end provides locally highly accurate camera poses and 3D reconstructions. Besides, the distribution of the points reconstructed by the VO is generally non-isotropic and highly dependent on the distance of an object point to the camera. Therefore, instead of performing global point cloud alignment, we use the provided ground truth poses to perform a keyframe-wise alignment between the camera-based reconstruction and the LiDAR ground truth. For all points hosted in a keyframe, we perform point matching in 2D by projecting the labeled

TABLE I: Evaluation results in per-class IoU and mIoU metrics of our approach on KITTI-360 dataset.

class	road	sidewalk	building	wall	fence	pole	traffic light	traffic sign	vegetation	terrain	car	truck	bus	train	motorcycle	bicycle	person	rider	mIoU
Baseline	94.4	79.4	86.6	54.6	34.4	39.2	6.6	45.7	90.1	60.8	83.4	71.7	89.1	91.8	46.3	19.3	36.2	4.0	58.5
TCL Mono	95.3	83.6	87.7	63.3	42.4	47.5	9.9	51.2	91.3	64.9	83.7	77.6	92.4	92.3	55.5	37.9	64.3	5.3	63.6
TCL Stereo	95.4	84.1	90.9	63.3	42.7	51.0	10.1	52.0	91.8	65.3	86.1	79.8	94.3	95.8	57.4	38.2	68.2	5.3	65.1

TABLE II: Evaluation results in class-wise mAcc and OA metrics of our approach on KITTI-360 dataset.

class	road	sidewalk	building	wall	fence	pole	traffic light	traffic sign	vegetation	terrain	car	truck	bus	train	motorcycle	bicycle	person	rider	OA
baseline	96.4	88.9	94.4	67.7	56.1	82.2	81.3	80.3	94.2	83.6	96.6	87.0	95.4	97.3	52.8	94.5	90.9	100.0	91.4
TCL Mono	97.3	91.2	94.7	73.0	58.1	83.8	87.3	83.2	95.5	85.8	97.9	93.3	96.3	97.3	62.4	95.8	94.0	100.0	94.1
TCL Stereo	97.5	91.9	95.1	73.2	59.9	84.5	87.6	83.4	95.6	85.8	98.2	93.4	98.5	98.9	64.8	97.0	94.6	100.0	95.2

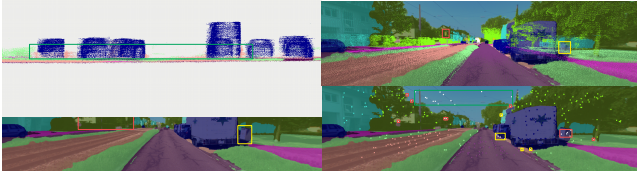


Fig. 4: **Label quality** of 3D and 2D semantic ground truth of the KITTI-360 dataset [1] and the semantic labels we associate for our point clouds. **Top Left:** In the *green* box, the points around the cars in *blue* are mislabeled as parking class in *pink* in KITTI-360 3D semantic ground truth. **Bottom Left:** In the *red* box, the building and traffic sign are mislabeled as vegetation and in the *yellow* box, a mail box is mislabeled as a car in KITTI-360 2D semantic ground truth. **Top Right:** The 3D semantic labels given by KITTI-360 projected into one keyframe where the traffic light and the mail box are not mislabeled. **Bottom Right:** The ground truth labels we associated for our point clouds based on the given KITTI-360 2D and 3D labels. The filtered points in *white*: the mislabeled points in *red* boxes, the points on the boundaries in *yellow* boxes, and the points in the sky in the *green* box.

LiDAR points into the keyframe image and assigning the labels of LiDAR points to the matched points. We utilize LiDAR points up to 100 meters away from the camera, which makes the projected points dense enough in 2D to have all points match a label. The top right plot in Figure 4 shows the density of the projected 3D points. Additionally, depth information is utilized to reject false assigned point pairs.

In KITTI-360 dataset, the labels of the 3D points are generated by placing primitive cuboids and ellipsoids around objects and assigning a class label to the enclosed points. Besides, it focuses on static scene objects. As a result, not all points are accurately labeled in 3D. The given 2D semantic ground truth is derived from the 3D labels, making the 2D ground truth not absolutely accurate as well. The left column of Figure 4 shows two examples that have mislabeled objects. Therefore, we fuse both the 2D image labels and the 3D LiDAR labels provided by the dataset to obtain reliable ground truth. Only if the labels of both 2D and projected 3D points are consistent, they are considered as ground truth for evaluation, as shown in the bottom right plot in Figure 4.

B. Evaluation

1) *Settings:* We evaluate our approach on all 9 released sequences of the KITTI-360 dataset. The evaluation is done on all classes as defined except the void-type classes, e.g. *unlabeled* and *ego vehicle*, etc., and the *sky* class as our map does not contain points representing the sky. The performance is evaluated for the baseline model presented in Section III-B [50] and the temporally consistent labeling

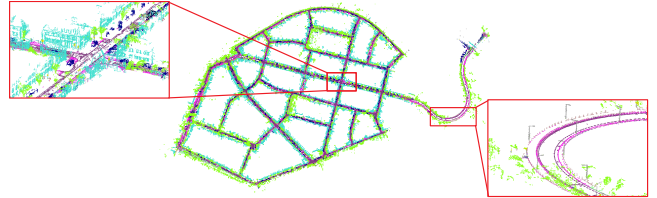


Fig. 5: **Large-scale semantic map** generated by the proposed pipeline. The figure shows the entire globally consistent reconstruction of Sequence 9 from the KITTI-360 dataset [1] and zoomed-in sections show the fine-grained reconstruction details.

(TCL) module based on the pre-trained network weights¹. For the TCL module we provide results using semantic labels predicted only for the left camera images (Mono) as well as using semantic labels for both left and right images (Stereo).

2) *Measurement Metric:* To evaluate the performance of semantic label prediction, we follow the standard to apply per-class intersection-over-union (IoU) [64] and the mean IoU (mIoU) metrics over all sequences.

$$IoU_c = \frac{TP_c}{TP_c + FP_c + FN_c} \quad mIoU = \frac{1}{C} \sum_{c=1}^C IoU_c \quad (4)$$

where TP_c , FP_c , and FN_c indicate the number of true positive, false positive, and false negative estimations for each class c in all sequences respectively. C is the number of evaluation classes.

As the number of points of each class varies prominently, we also measure the class-wise prediction mean accuracy (mAcc) and the overall accuracy (OA) over all sequences:

$$mAcc = \frac{TP_c}{N_c} \quad OA = \frac{\sum_{c=1}^C TP_c}{\sum_{c=1}^C N_c} \quad (5)$$

where N_c is the number of points predicted as class c .

3) *Results:* Table I shows the evaluation results in per-class IoU and mIoU. Table II presents them in class-wise mAcc and OA. These class-wise measurements indicate that our approach performs well on primary static classes, including road, sidewalk, building and vegetation classes, and also on some dynamic classes, car, truck, and bus because most objects of these classes are not moving in these sequences. When comparing Table I and Table II, we can conclude that our approach performs better in terms of precision than recall, especially on classes representing small

¹<https://github.com/NVIDIA/semantic-segmentation/tree/sdcnet>



Fig. 6: **Semantic point labels generated by our approach.** The sparse points hosted in a keyframe are overlaid with the 2D ground truth labels and the image from KITTI-360. This is only a subset of all points in the optimization window. Two rows represent one example, where the first and second row shows the prediction results in full images and the zoom-in windows, respectively. Columns show (*left*) sparse ground truth labels, (*center*) labels predicted by the baseline model, (*right*) labels estimated by TCL, respectively. Points which are wrongly predicted by the baseline but corrected by the TCL are highlighted with *green* boxes. Points not corrected by the TCL are highlighted with *red* boxes.

objects, e.g. traffic sign, traffic light, bicycle, person. These small objects have more complex and elongated boundaries, and the points near boundaries are more challenging to be perfectly classified. Besides, there are only a few points corresponding to the small objects, and thus a wrong prediction can reduce the IoU and mAcc by a large margin. Thus, the large classes has better results than the small classes.

The proposed temporally consistent labeling (TCL) fixes inconsistent predictions which mainly occur on object boundaries across consecutive frames. Therefore, TCL outperforms the baseline model, especially on small objects, e.g. pole, motorcycle, bicycle, and person. Furthermore, the stereo version clearly outperforms the mono version.

Qualitative results of semantic point cloud labels generated by our approach are shown in Figure 6. It illustrates how TCL can improve the label estimation accuracy. Additionally, Figure 5 shows an entire large-scale map generated by our approach from the sequence 9 in KITTI-360 dataset.

V. CONCLUSION

We presented a large-scale semantic mapping pipeline, which combines a state-of-the-art direct sparse VO front-end and a back-end with global optimization and image-based semantic segmentation. We demonstrated that predictions of the semantic segmentation network could be improved by incorporating temporal correspondences established by VO. Furthermore, we showed that our pipeline is capable of generating city-scale semantic maps covering thousands of kilometers of the road by using a fleet of vehicles. Such large-scale semantic maps can serve as intermediate results towards fully vectorized HD maps. Besides, we see it as a next step to build semantic 3D volumetric maps at scale with the combination of state-of-the-art dense reconstruction approaches like [65].

ACKNOWLEDGEMENT

We thank the entire Artisense team for their support in setting up the pipeline and making this project happen.

REFERENCES

- [1] J. Xie, M. Kiefel, M.-T. Sun, and A. Geiger, "Semantic instance annotation of street scenes by 3D to 2D label transfer," in *IEEE Conference on Computer Vision and Pattern Recognition (CVPR)*, 2016.
- [2] A. Geiger, P. Lenz, and R. Urtasun, "Are we ready for autonomous driving? the KITTI vision benchmark suite," in *IEEE Conference on Computer Vision and Pattern Recognition (CVPR)*, 2012.
- [3] M. Cordts, M. Omran, S. Ramos, T. Rehfeld, M. Enzweiler, R. Benenson, U. Franke, S. Roth, and B. Schiele, "The cityscapes dataset for semantic urban scene understanding," in *IEEE Conference on Computer Vision and Pattern Recognition (CVPR)*, 2016.
- [4] G. Neuhold, T. Ollmann, S. Rota Bulò, and P. Kotschieder, "The mapillary vistas dataset for semantic understanding of street scenes," in *International Conference on Computer Vision (ICCV)*, 2017.
- [5] J. Behley, M. Garbade, A. Milioto, J. Quenzel, S. Behnke, C. Stachniss, and J. Gall, "SemanticKITTI: A dataset for semantic scene understanding of lidar sequences," in *International Conference on Computer Vision (ICCV)*, 2019.
- [6] P. Wang, X. Huang, X. Cheng, D. Zhou, Q. Geng, and R. Yang, "The apolloscape open dataset for autonomous driving and its application," *IEEE Transactions on Pattern Analysis and Machine Intelligence (TPAMI)*, 2019.
- [7] P. Wenzel, R. Wang, N. Yang, Q. Cheng, Q. Khan, L. von Stumberg, N. Zeller, and D. Cremers, "4Seasons: A cross-season dataset for multi-weather SLAM in autonomous driving," in *German Conference on Pattern Recognition (GCPR)*, 2020.
- [8] G. Klein and D. Murray, "Parallel tracking and mapping for small AR workspaces," in *IEEE and ACM International Symposium on Mixed and Augmented Reality (ISMAR)*, 2007.
- [9] R. Mur-Artal, J. M. M. Montiel, and J. D. Tardós, "ORB-SLAM: a versatile and accurate monocular SLAM system," *IEEE Transactions on Robotics (T-RO)*, 2015.
- [10] R. Mur-Artal and J. D. Tardós, "ORB-SLAM2: An open-source SLAM system for monocular, stereo and RGB-D cameras," *IEEE Transactions on Robotics (T-RO)*, 2017.
- [11] R. Elvira, J. M. M. Montiel, and J. D. Tardós, "ORB-SLAM-Atlas: A robust and accurate multi-map system," in *IEEE/RSJ International Conference on Intelligent Robots and Systems (IROS)*, 2019.
- [12] V. Usenko, N. Demmel, D. Schubert, J. Stückler, and D. Cremers, "Visual-inertial mapping with non-linear factor recovery," *IEEE Robotics and Automation Letters (RA-L)*, 2020.
- [13] C. Campos, R. Elvira, J. J. Gómez Rodríguez, J. M. M. Montiel, and J. D. Tardós, "ORB-SLAM3: An accurate open-source library for visual, visual-inertial and multi-map SLAM," *IEEE Transactions on Robotics (T-RO)*, 2021.
- [14] R. Mur-Artal and J. D. Tardós, "Probabilistic semi-dense mapping from highly accurate feature-based monocular SLAM," in *Robotics: Science and Systems (RSS)*, 2015.
- [15] T. Schöps, T. Sattler, C. Häne, and M. Pollefeys, "3D modeling on the go: Interactive 3D reconstruction of large-scale scenes on mobile devices," in *International Conference on 3D Vision (3DV)*, 2015.
- [16] J. L. Schönberger, E. Zheng, M. Pollefeys, and J.-M. Frahm, "Pixel-wise view selection for unstructured multi-view stereo," in *European Conference on Computer Vision (ECCV)*, 2016.
- [17] J. Engel, T. Schöps, and D. Cremers, "LSD-SLAM: Large-scale direct monocular SLAM," in *European Conference on Computer Vision (ECCV)*, 2014.
- [18] J. Engel, V. Koltun, and D. Cremers, "Direct sparse odometry," *IEEE Transactions on Pattern Analysis and Machine Intelligence (TPAMI)*, 2018.
- [19] R. Wang, M. Schwörer, and D. Cremers, "Stereo DSO: Large-scale direct sparse visual odometry with stereo cameras," in *International Conference on Computer Vision (ICCV)*, 2017.
- [20] N. Yang, L. von Stumberg, R. Wang, and D. Cremers, "D3VO: Deep depth, deep pose and deep uncertainty for monocular visual odometry," in *IEEE Conference on Computer Vision and Pattern Recognition (CVPR)*, 2020.
- [21] X. Gao, R. Wang, N. Demmel, and D. Cremers, "LDSO: Direct sparse odometry with loop closure," in *IEEE/RSJ International Conference on Intelligent Robots and Systems (IROS)*, 2018.
- [22] M. Gladkova, R. Wang, N. Zeller, and D. Cremers, "Tight integration of feature-based relocalization in monocular direct visual odometry," in *IEEE International Conference on Robotics and Automation (ICRA)*, 2021.
- [23] J. L. Schönberger and J.-M. Frahm, "Structure-from-motion revisited," in *IEEE Conference on Computer Vision and Pattern Recognition (CVPR)*, 2016.
- [24] N. Demmel, M. Gao, E. Laude, T. Wu, and D. Cremers, "Distributed photometric bundle adjustment," in *International Conference on 3D Vision (3DV)*, 2020.
- [25] J. Long, E. Shelhamer, and T. Darrell, "Fully convolutional networks for semantic segmentation," in *IEEE Conference on Computer Vision and Pattern Recognition (CVPR)*, 2015.
- [26] H. Zhao, J. Shi, X. Qi, X. Wang, and J. Jia, "Pyramid scene parsing network," in *IEEE Conference on Computer Vision and Pattern Recognition (CVPR)*, 2017.
- [27] L.-C. Chen, G. Papandreou, F. Schroff, and H. Adam, "Rethinking atrous convolution for semantic image segmentation," in *IEEE Conference on Computer Vision and Pattern Recognition (CVPR)*, 2017.
- [28] L.-C. Chen, G. Papandreou, I. Kokkinos, K. Murphy, and A. Yuille, "Semantic image segmentation with deep convolutional nets and fully connected crfs," in *International Conference on Learning Representations (ICLR)*, 2015.
- [29] A. Schwing and R. Urtasun, "Fully connected deep structured networks," *ArXiv*, 2015.
- [30] S. Zheng, S. Jayasumana, B. Romera-Paredes, V. Vineet, Z. Su, D. Du, C. Huang, and P. H. S. Torr, "Conditional random fields as recurrent neural networks," in *International Conference on Computer Vision (ICCV)*, 2015.
- [31] G. Lin, C. Shen, A. van den Hengel, and I. Reid, "Efficient piecewise training of deep structured models for semantic segmentation," in *IEEE Conference on Computer Vision and Pattern Recognition (CVPR)*, 2016.
- [32] D. Eigen and R. Fergus, "Predicting depth, surface normals and semantic labels with a common multi-scale convolutional architecture," in *International Conference on Computer Vision (ICCV)*, 2015.
- [33] L.-C. Chen, Y. Yang, J. Wang, W. Xu, and A. Yuille, "Attention to scale: Scale-aware semantic image segmentation," in *IEEE Conference on Computer Vision and Pattern Recognition (CVPR)*, 2016.
- [34] C. Farabet, C. Couprie, L. Najman, and Y. LeCun, "Learning hierarchical features for scene labeling," *IEEE Transactions on Pattern Analysis and Machine Intelligence (TPAMI)*, 2013.
- [35] P. H. O. Pinheiro and R. Collobert, "Recurrent convolutional neural networks for scene labeling," in *International Conference on Machine Learning (ICML)*, 2014.
- [36] L.-C. Chen, G. Papandreou, I. Kokkinos, K. Murphy, and A. Yuille, "DeepLab: Semantic image segmentation with deep convolutional nets, atrous convolution, and fully connected crfs," *IEEE Transactions on Pattern Analysis and Machine Intelligence (TPAMI)*, 2018.
- [37] H. Zhao, J. Shi, X. Qi, X. Wang, and J. Jia, "Pyramid scene parsing network," in *IEEE Conference on Computer Vision and Pattern Recognition (CVPR)*, 2017.
- [38] W. Liu, A. Rabinovich, and A. Berg, "ParseNet: Looking wider to see better," *ArXiv*, 2015.
- [39] H. Noh, S. Hong, and B. Han, "Learning deconvolution network for semantic segmentation," in *International Conference on Computer Vision (ICCV)*, 2015.
- [40] V. Badrinarayanan, A. Kendall, and R. Cipolla, "SegNet: A deep convolutional encoder-decoder architecture for image segmentation," *IEEE Transactions on Pattern Analysis and Machine Intelligence (TPAMI)*, 2017.
- [41] O. Ronneberger, P. Fischer, and T. Brox, "U-Net: Convolutional networks for biomedical image segmentation," in *miccai*, 2015.
- [42] G. Lin, A. Milan, C. Shen, and I. Reid, "RefineNet: Multi-path refinement networks for high-resolution semantic segmentation," in *IEEE Conference on Computer Vision and Pattern Recognition (CVPR)*, 2017.
- [43] T. Pohlen, A. Hermans, M. Mathias, and B. Leibe, "Full-resolution residual networks for semantic segmentation in street scenes," in *IEEE Conference on Computer Vision and Pattern Recognition (CVPR)*, 2017.
- [44] J. Fu, J. Liu, Y. Wang, and H. Lu, "Stacked deconvolutional network for semantic segmentation," *IEEE Transactions on Image Processing*, 2017.
- [45] J. Fu, J. Liu, H. Tian, Z. Fang, and H. Lu, "Dual attention network for scene segmentation," in *IEEE Conference on Computer Vision and Pattern Recognition (CVPR)*, 2019.
- [46] Z. Huang, X. Wang, L. Huang, C. Huang, Y. Wei, H. Shi, and

- W. Liu, "CCNet: Criss-cross attention for semantic segmentation," in *International Conference on Computer Vision (ICCV)*, 2019.
- [47] Y. Yuan, L. Huang, J. Guo, C. Zhang, and X. Chen, "OCNet: Object context for semantic segmentation," *International Journal of Computer Vision (IJCV)*, 2021.
- [48] A. Tao, K. Sapra, and B. Catanzaro, "Hierarchical multi-scale attention for semantic segmentation," *ArXiv*, 2020.
- [49] C. Yu, J. Wang, C. Peng, C. Gao, G. Yu, and N. Sang, "Learning a discriminative feature network for semantic segmentation," in *IEEE Conference on Computer Vision and Pattern Recognition (CVPR)*, 2018.
- [50] Y. Zhu, K. Sapra, F. A. Reda, K. J. Shih, S. Newsam, A. Tao, and B. Catanzaro, "Improving semantic segmentation via video propagation and label relaxation," in *IEEE Conference on Computer Vision and Pattern Recognition (CVPR)*, 2019.
- [51] A. Iscen, G. Toliás, Y. Avrithis, and O. Chum, "Label propagation for deep semi-supervised learning," in *IEEE Conference on Computer Vision and Pattern Recognition (CVPR)*, 2019.
- [52] Y. Zou, Z. Yu, B. V. Kumar, and J. Wang, "Unsupervised domain adaptation for semantic segmentation via class-balanced self-training," in *European Conference on Computer Vision (ECCV)*, 2018.
- [53] Y. Li, L. Yuan, and N. Vasconcelos, "Bidirectional learning for domain adaptation of semantic segmentation," in *IEEE Conference on Computer Vision and Pattern Recognition (CVPR)*, 2019.
- [54] B. Wu, A. Wan, X. Yue, and K. Keutzer, "SqueezeSeg: Convolutional neural nets with recurrent CRF for real-time road-object segmentation from 3D LiDAR point cloud," in *IEEE International Conference on Robotics and Automation (ICRA)*, 2018.
- [55] Y. Wang, T. Shi, P. Yun, L. Tai, and M. Liu, "PointSeg: Real-time semantic segmentation based on 3D lidar point cloud," 2018.
- [56] L. Tchammi, C. Choy, I. Armeni, J. Gwak, and S. Savarese, "SEG-Cloud: Semantic segmentation of 3D point clouds," in *International Conference on 3D Vision (3DV)*, 2017.
- [57] S. Sengupta, P. Sturgess, L. Ladicky, and P. H. S. Torr, "Automatic dense visual semantic mapping from street-level imagery," in *IEEE/RSJ International Conference on Intelligent Robots and Systems (IROS)*, 2012.
- [58] S. Sengupta, E. Greveson, A. Shahrokni, and P. H. S. Torr, "Urban 3D semantic modelling using stereo vision," in *IEEE International Conference on Robotics and Automation (ICRA)*, 2013.
- [59] I. Kostavelis and A. Gasteratos, "Semantic mapping for mobile robotics tasks: A survey," *Robotics and Autonomous Systems*, 2015.
- [60] D. Maturana, P.-W. Chou, M. Uenoyama, and S. Scherer, "Real-time semantic mapping for autonomous off-road navigation," in *International Conference on Field and Service Robotics (FSR)*, 2017.
- [61] D. Paz, H. Zhang, Q. Li, H. Xiang, and H. I. Christensen, "Probabilistic semantic mapping for urban autonomous driving applications," in *IEEE/RSJ International Conference on Intelligent Robots and Systems (IROS)*. IEEE, oct 2020.
- [62] L. von Stumberg, V. Usenko, and D. Cremers, "Direct sparse visual-inertial odometry using dynamic marginalization," in *IEEE International Conference on Robotics and Automation (ICRA)*, 2018.
- [63] H. Alhaija, S. Mustikovela, L. Mescheder, A. Geiger, and C. Rother, "Augmented reality meets computer vision: Efficient data generation for urban driving scenes," *International Journal of Computer Vision (IJCV)*, 2018.
- [64] M. Everingham, S. M. Eslami, L. Gool, C. K. Williams, J. Winn, and A. Zisserman, "The pascal visual object classes challenge: A retrospective," in *International Journal of Computer Vision (IJCV)*, 2015.
- [65] F. Wimbauer, N. Yang, L. von Stumberg, N. Zeller, and D. Cremers, "MonoRec: Semi-supervised dense reconstruction in dynamic environments from a single moving camera," in *IEEE Conference on Computer Vision and Pattern Recognition (CVPR)*, 2021.